Biomedical Signal Processing and Control 45 (2018) 225–236

Contents lists available at ScienceDirect

Biomedical Signal Processing and Control

journal homepage: www.elsevier.com/locate/bspc

Novel electromyography signal envelopes based on binary segmentation

J.A. Guerrero [a], M.A. Castillo-Galván [b], J.E. Macías-Díaz [c,*]

[a] Departamento de Estadística, Universidad Autónoma de Aguascalientes, Avenida Universidad 940, Ciudad Universitaria, Aguascalientes, Ags. 20131, Mexico
[b] Centro de Ciencias Básicas, Universidad Autónoma de Aguascalientes, Avenida Universidad 940, Ciudad Universitaria, Aguascalientes, Ags. 20131, Mexico
[c] Departamento de Matemáticas y Física, Universidad Autónoma de Aguascalientes, Avenida Universidad 940, Ciudad Universitaria, Aguascalientes, Ags. 20131, Mexico

ARTICLE INFO

Article history:
Received 17 August 2017
Received in revised form 23 March 2018
Accepted 28 May 2018

MSC:
62M10
62P10
62F10

Keywords:
Electromyography signal
Envelope
Binary segmentation
Change-points

ABSTRACT

In this work, we introduce two novel methodologies to compute the envelope of superficial electromyography signals. Our methods are based on the detection of activation and deactivation patterns using a change-point approach on the variances of the sample. More concretely, an iterative algorithms is proposed to select the change-points between two segments of the signal based on some local statistics introduced in this work. The signal is split up into two segments, and a new search for change-points is recursively conducted in each subsequence. The change-points make possible to calculate local envelopes which reflect the shape of the signal without ignoring the activation and deactivation landmarks. Two methods are proposed in this work, and the improvements with respect to methodologies available in the literature are shown using both synthetic and real data. A thorough analysis of the techniques is performed to that end.

1. Introduction

Electromyography (EMG) signals are an important topic of active research in view of their wide range of medical applications. For example, EMG signals have been classified using different criteria in order to diagnose neuromuscular disorders [1], they have been used as a tool in the evaluation of generalized tonic–clonic seizure semiology [2], in the recognition of emotions using facial recordings and statistical methods [3], in the automatic control of upper limb prosthesis [4], as a criterion to determine the differences in lower-extremity muscular activation walking between older and young adults [5], in the investigation of neck and shoulder muscle activity of orthodontists in natural environments [6] and as a mechanism to measure shoulder muscle fatigue during repetitive tasks [7] among other interesting biomedical applications.

It is important to recall that EMG signals are measurements of the difference of electric potentials between two electrodes. In turn, these measurements are highly correlated to the intensity in muscular activity [8]. There are various well-established procedures to record EMG signals, one of them is called superficial electromyography (sEMG), which consists in placing the electrodes over the skin covering the muscle of interest using a conductive gel to get better data readings [9]. An sEMG signal is essentially a random stationary temporal series in which the activity of the measured muscle is reflected as an increase in the signal amplitude (also called a 'burst' in this work). Muscular activity may be identified by finding the localization, duration, shape and amplitude of those bursts in the electric signal.

Beforehand we must recall that there are various approaches to investigate EMG signals from an automatic point of view. For instance, the recent literature shows progresses on de-noising techniques to remove electric interferences in EMG signals [10], on the efficient decision-tree algorithms for the classification of EMG signals using the discrete wavelet transform [11], on the use of two-directional two-dimensional principal component analysis based on stationary wavelets for EMG signals [12] and on the detection of activation/deactivation patterns in EMG signals with two [13] or more levels of electric activity [14]. However, the methods have sometimes limited applicability, and there are still many

* Corresponding author.
E-mail addresses: macastillo@correo.uaa.mx (M.A. Castillo-Galván), jemacias@correo.uaa.mx (J.E. Macías-Díaz).

https://doi.org/10.1016/j.bspc.2018.05.026
1746-8094/

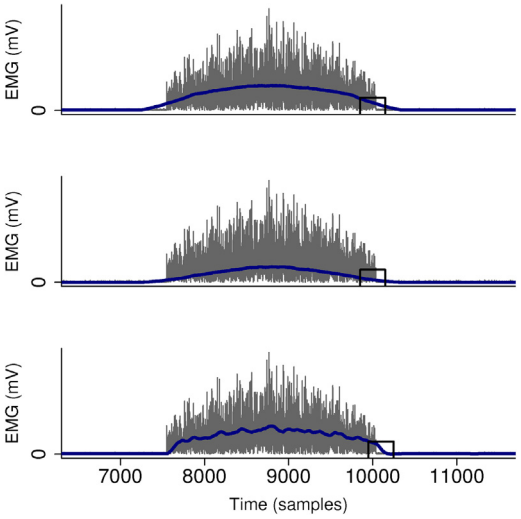

Fig. 1. Envelopes for the same EMG signal calculated using moving averages (top), root-mean squares (middle) and the Butterworth low-pass filter (bottom). The signal is depicted in gray while the calculated envelope is shown as a thick dark blue line. In all three cases, the black rectangles around sample 10,000 show failures of the methods in the detection of the end of a burst. (For interpretation of the references to color in text/this figure legend, the reader is referred to the web version of the article.)

open problems in the development of robust methodologies for the investigation of EMG signals.

As an example on the limitations of some of the methodologies available in the literature, recall that one way to recover the signal burst shape is by computing its envelope. The most common methods to compute envelopes are using moving averages [15,16], root-mean squares [17,18] and Butterworth low-pass filters [19,20]. However, it is important to point out that these methods lack effectiveness in detecting the beginning and the end of the bursts, and that this problem becomes more evident when one tries to obtain a smooth envelope. More concretely, this shortcoming appears when the window size is increased in the case of moving averages or root-mean squares, and when the cut frequency is decreased in the case of Butterworth low-pass filters.

For illustration purposes, Fig. 1 shows the limitations inherent to the calculation of envelopes using moving averages (top), root-mean squares (middle) and the Butterworth low-pass filter (bottom). In that figure, envelopes were calculated for the same EMG signal using the procedures described above. The signal is shown in gray while the envelope is depicted in dark blue. The black rectangles enhance the points of the temporal series where the methods fail to detect correctly the end of an activation period. Obviously, this is a strong limitation of these techniques which merits a closer attention.

In the present work, we will propose two methodologies to compute the envelope of an EMG signal for which the start and the end of the burst do not vanish. As some papers available in the literature [21,22], our approach will be based on the calculation of statistics that are computed 'locally' around the points in the signal. The notion of locality in our context will hinge basically on suitable neighborhoods of points for which the variance has no statistical difference. In order to identify segments in the temporal series with similar variance we will employ an iterative algorithm to detect all the change-points on the variances. Some illustrative simulations will establish the effectiveness of the proposed methodology.

This paper is organized as follows. Section 2 introduces the nomenclature employed throughout this work along with the change-point model proposed and the corresponding statistical hypotheses. In turn, Section 3 will be devoted to develop an iterative algorithm based on the change-point model. In Section 4 we show some illustrative simulations using both experimental and synthetic EMG signals. For the sake of a more objective comparison, we will contrast the performance of the proposed method against others envelope techniques available in the literature. We close this manuscript with a section of final remarks.

2. Mathematical model

Let n be a positive integer. Throughout we let $x = \{x_i\}_{i=1}^n \subseteq \mathbb{R}$ be a finite sequence which physically represents a sEMG signal (an EMG for short). More precisely, x_i is a sample of the myoelectric activity of a muscle recorded at the time t_i for each $i \in \{1, \ldots, n\}$. For practical purposes, the sequence $\{t_i\}_{i=1}^n$ may represent a uniform partition of the temporal interval $[0, T]$ with $T > 0$. For each $i \in \{1, \ldots, n\}$ let X_i be a normally distributed random variable with mean equal to zero and variance equal to σ_i^2, that is,

$$X_i \sim N(0, \sigma_i^2), \quad \forall i \in \{1, \ldots, N\}. \tag{1}$$

In this work, we will suppose that x is a sample of the sequence of random variables $X = \{X_1, \ldots, X_n\}$.

In this section, we propose a change-point model for the variances of the signal in order to describe different activity levels of x. Our approach hinges on the hypothesis that there exists $M \in \mathbb{N}$ as well as integer numbers

$$0 < k_1 < \cdots < k_{M+1} = n, \tag{2}$$

called *change-points*. Moreover, we will suppose that the variance is constant between two consecutive change-points, and that it changes at each of them. Mathematically,

$$\begin{cases} \mathbf{H}_0: & \sigma_i^2 = \sigma_{k_j}^2, \quad \forall k_j \le i < k_{j+1}, \forall j \in \{1, \ldots, M-1\}, \\ \mathbf{H}_1: & \sigma_{k_j}^2 \neq \sigma_{k_{j+1}}^2, \quad \forall j \in \{1, \ldots, M-1\}. \end{cases} \tag{3}$$

It is worth noting that, in practice, the number of change-points and their locations are not known *a priori*. In order to propose a methodology to determine them, we consider firstly the case of a single point (that is, when $M = 1$) and two possible scenarios: when the location is know or unknown. In a second stage, we will propose an algorithm based on two new local statistics for the general case when $M \in \mathbb{N}$. All of this possibilities will be considered next.

2.1. One change-point with known location

Suppose that there is only one change-point, and assume that its possible location is $k \in \{2, \ldots, n\}$. Throughout we let $\sigma_{k,L}^2$ represent the common variance of the left subsequence $\{X_1, X_2, \ldots, X_{k-1}\}$, and let $\sigma_{k,R}^2$ denote the common variance of the right subsequence $\{X_k, X_{k+1}, \ldots, X_n\}$. In order to determine whether there is a significant change in the variance at the time t_k, the respective set of null and alternative hypotheses is given by

$$\begin{cases} \mathbf{H}_0: & \sigma_{k,L}^2 = \sigma_{k,R}^2, \\ \mathbf{H}_1: & \sigma_{k,L}^2 \neq \sigma_{k,R}^2. \end{cases} \tag{4}$$

The test statistic for the likelihood-ratio test is given by

$$\begin{aligned} D_k &= -2 \ln \Lambda_k \\ &= 2[n \ln(\hat{\sigma}^2) - k \ln(\hat{\sigma}_{k,L}^2) - (n - k + 1) \ln(\hat{\sigma}_{k,R}^2)], \end{aligned} \tag{5}$$

where Λ_k is the likelihood ratio:

$$\Lambda_k = \frac{\sup_{\sigma^2} L_0(\sigma^2|x)}{\sup_{\sigma^2_{k,L},\sigma^2_{k,R}} L_1(\sigma^2_{k,L},\sigma^2_{k,R}|x)} = \frac{L_0(\hat{\sigma^2}|x)}{L_1(\hat{\sigma^2}_{k,L},\hat{\sigma^2}_{k,R}|x)}. \tag{6}$$

Here L_0 and L_1 are the likelihood under H_0 and H_1, respectively. Moreover, under the assumption that all the variables involved have a mean equal to zero, the estimators

$$\hat{\sigma}^2 = \frac{1}{n}\sum_{i=1}^{n} x_i^2, \tag{7}$$

$$\hat{\sigma}^2_{k,L} = \frac{1}{k-1}\sum_{i=1}^{k-1} x_i^2, \tag{8}$$

$$\hat{\sigma}^2_{k,R} = \frac{1}{n-k+1}\sum_{i=k}^{n} x_i^2, \tag{9}$$

are respectively the maximum likelihood estimators of σ^2 under H_0, and of $\sigma^2_{k,L}$ and $\sigma^2_{k,R}$ under H_1. It is worth noting that D_k is asymptotically χ^2-distributed with one degree of freedom [23].

2.2. One change-point with unknown location

Consider the following test for a significant change in the variance with no assumptions on the location of the possible change-point:

$$\begin{cases} \mathbf{H_0}: & \sigma_k^2 = \sigma^2, \quad \forall k \in \{1,\ldots,n\}, \\ \mathbf{H_1}: & \exists k^* \in J_n \text{ such that} \\ & \sigma_1^2 = \cdots = \sigma^2_{k^*-1} \neq \sigma^2_{k^*} = \cdots = \sigma_n^2. \end{cases} \tag{10}$$

The test statistic that considers all the possible locations for a single change-point is

$$D = \max_{k=1,\ldots,n} D_k. \tag{11}$$

Note that the determination of the distribution of D is a difficult task in view that the statistics $D_1, \ldots, D_n$ are not uncorrelated. In the present case, an approximation to the critical point of $\sqrt{D}$ for a level of significance equal to α is the largest value x that solves the equation

$$\frac{xe^{-x^2/2}}{\sqrt{2\pi}}\left[\left(1-\frac{1}{x^2}\right)\log\frac{\left(1-(\log n)^{3/2}/n\right)^2}{\left((\log n)^{3/2}/n\right)^2}+\frac{4}{x^2}\right] = \alpha. \tag{12}$$

For more details, we refer to [24].

2.3. Multiple change-points. Unknown locations

Finally, consider the general case in which there may be various change-points with unknown locations. In this case the associated null and alternative hypotheses are

$$\begin{cases} \mathbf{H_0}: & \sigma_k^2 = \sigma^2, \quad \forall k \in \{1.\ldots.n\}, \\ \mathbf{H_1}: & \exists M \in \mathbb{N} \text{ and } 1 < k_1 < \cdots < k_{M+1} = n \text{ such that} \\ & \sigma_1^2 = \ldots = \sigma^2_{k_1-1} \neq \sigma^2_{k_1} = \ldots = \sigma^2_{k_2-1} \neq \\ & \ldots \neq \sigma^2_{k_M} = \ldots = \sigma_n^2. \end{cases} \tag{13}$$

For this general scenario, we describe next an iterative algorithm to find all the possible change-point locations.

3. Methodology

3.1. Iterative technique

Throughout this section, we will consider the problem described in Section 2.3. Our approach will be based on a hierarchical splitting method from cluster analysis in which groups are split up into two subgroups based on homogeneity criteria [25]. In turn, such procedure will be applied to each subgroup separately until the resulting subgroups are homogeneous.

Using the method proposed in [25] and (11), the first step is to find the best guesses for a single change-point on the entire data, including those points that may not be statistically significant. These values are stored for further consideration and, for each of them, the signal is divided into two subsequences at the change-point location. In each case, each of the subsequences is treated as a separate sequence, and the procedure is repeated until all the subsequences consist of a single sample point.

In order to get rid of those change-points which are not statistically significant, all the values of the statistic D are tested against the corresponding solution of (12). It is important not to test the significance of the change-points during the splitting iterative procedure. This is due to the fact that there are special cases when a sequence can be divided into two subsequences with no significant differences in variance, but they may contain change-points inside them. As an example, consider an EMG signal that begins and ends with a phase of activity, but contains a small phase of inactivity in the middle. In such signal, there may not exist any point that divides the signal into two segments of different variance. Indeed, any possible change-point will have many sample points of phases of activity on the two associated segments.

3.2. Local statistics

The techniques of moving averages and root-mean square hinge on the calculation of local statistics using a moving window for all points. For instance, to calculate the envelope for a point $i \in \{1,\ldots,n\}$ the following formula is used:

$$MA(i) = \frac{\sum_{w\in W_i} Y(w)}{|W_i|}, \tag{14}$$

where

$$W_i = \left\{j : |j-i| \leq k\right\} \tag{15}$$

is a moving window of length equal to k, $|W_i| \in \left\{1,\ldots,2k+1\right\}$ is the number of elements in W_i and Y is the rectified signal $Y(i) = |X(i)|$. It is worth noting that using $X(w)$ instead of $Y(w)$ would result in values approximately equal to zero for each $i \in \{1,\ldots,n\}$. This is due to the fact that the EMG signals oscillate naturally around 0.

In order to identify the start and end of a burst in the signal, we consider $M+1$ segments using M detected change-points. Let $SEG(i)$ be the index for the ith point which belongs to that segment. It is obvious that $SEG(i) \in \left\{1,\ldots,M+1\right\}$. The proposed improvement for the moving average envelope is defined as follows:

$$MAbs(i) = \frac{\sum_{w\in \hat{W}_i} Y(w)}{|\hat{W}_i|}. \tag{16}$$

Here

$$\hat{W}_i = \left\{j : SEG(i) = SEG(j) \text{ and } |j-i| \leq k\right\}. \tag{17}$$

Note that the neighborhood at the ith point only takes into account the points which belongs to the same segment of the signal. Similarly, it is possible to calculate local standard deviations

(recall that a mean equal to zero is assumed for the whole signal) through

$$SDsb(i) = \sqrt{\frac{\sum_{w \in \hat{W}_i} X^2(w)}{|\hat{W}_i|}}. \quad (18)$$

These standard deviations allow to calculate the upper limit of a confidence interval on each point of the signal:

$$CIbs(i) = \bar{X}_i + z_{0.05} SDsb(i). \quad (19)$$

Here $z_{0.05}$ is the 0.05 quantile of the standard normal distribution and

$$\bar{X}_i = \sqrt{\frac{\sum_{w \in \hat{W}_i} X(w)}{|\hat{W}_i|}}. \quad (20)$$

Note that $\bar{X}_i \neq MAbs(i)$ because the latter uses the rectified signal Y instead of X.

4. Results

The following experiments show the effects of the envelope parameters on synthetic and real signals. Likewise, they show the capability of the new algorithms introduced in Section 3 to retrieve the shape and the bursts of the signal. In order to show quantitatively the performance of the methodology, we opted to use synthetic signals. In this way, the characteristics of the signals (especially the exact location of the activity phases) were known before the envelope was computed.

The synthetic signals employed in this section were obtained as the juxtaposition of phases of activity and silence. The phases of silence were constructed as random samples of a normal distribution with mean equal to zero and variance σ_s^2. Each of the activity phases was constructed as follows:

- The variances of the random samples satisfy $\sigma_a > \sigma_n$. Thee values determine the signal-to-noise ration (SNR), which is defined in decibels (dB) by

$$SNR = 20\log_{10}\left(\frac{\sigma_a}{\sigma_s}\right). \quad (21)$$

- A shape curve S_{shape} with values between 0 and 1 was produced. This curve determines the shape of the activity phase with the same length as S_A. For illustration purposes, Fig. 6 shows the forms of the activity phases obtained for three different shape curves.
- The curve S_A was multiplied by the shape curve S_{shape}.
- Finally, we applied a Butterworth filter to all the signals using a cut-off frequency of 20 Hz. This process was performed in order to obtain signals with frequency ranges similar to those of the real EMG signals.

4.1. Simulations

Example 1. Effect of α and window size: The effects of the parameter α on the detection of change-points may be noted in Fig. 2. Indeed, with small values of α only big differences of the variance between the segments will prevail after the statistical test. Meanwhile large values of α allow for more segmentation, as expected. This is because the segments are statistically different in spite that they are apparently similar. As conclusion, the parameter α can be used to control the size of the jumps allowed in the envelope. As it happens with the methods of moving averages and root-mean squares, the window size smooths the envelope. This fact is illustrated in Fig. 3. Note that the same effect occurs with the methods presented in this work, taking into account the change-points of the signal. As a conclusion, by adjusting both parameters it is possible to control the details (peaks and valleys) of the envelope.

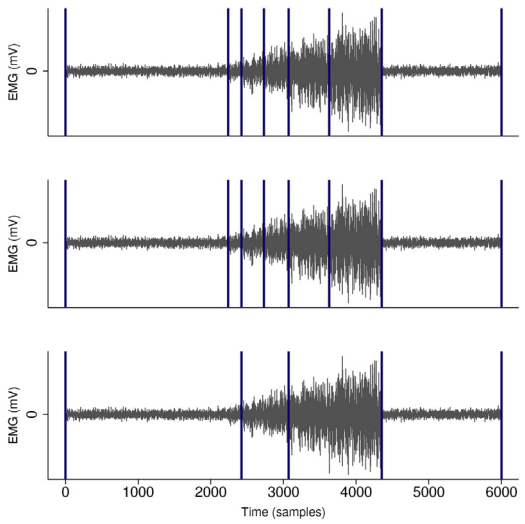

Fig. 2. Effect of the parameter α on the change-points detected by the binary segmentation. The blue lines are the detected change-points of the variance using the values $\alpha = 0.10$ (top), $\alpha = 1 \times 10^{-10}$ (middle) and 1×10^{-50} (bottom). (For interpretation of the references to color in text/this figure legend, the reader is referred to the web version of the article.)

Example 2 *(Shape recovery).* Figs. 4 and 5 illustrate how the algorithm can retrieve the shape of the burst in the signal. To that end, synthetic EMG signals with different shapes were considered. The envelopes were computed using five methods. More precisely, Fig. 4 shows the results obtained using (a) moving averages, (b) *MAbs*, (c) root-mean squares and (d) *CIbs* for a window size $w = 50$; meanwhile Fig. 5 is obtained using the Butterworth lower-pass filter with a cut frequency equal to 60 Hz. Note that the shape vanishes using moving averages and root-mean squares, while the methods *CIbs* and *MAbs* both retrieve shape. Moreover, *CIbs* can also retrieve the amplitude of the signal.

4.2. Manual selection

4.2.1. Methodology

The purpose of this section is to show that the proposed envelopes are capable of assisting in the manual selection of beginning and ending points of activation phases. Nowadays, there are researchers who select manually the change of phases, mainly due to the lack of reliable automatic methods for the analysis of EMG signals. The experiment of this section was carried out under the following methodology.

Subjects. Seven students of the Universidad Autónoma de Aguascalientes (UAA) participated in the manual selection of beginning and ending points of phases. The group consisted of

- 4 female and 3 male students,
- 3 were undergraduate and 4 were graduate students,
- 1 was an expert in manual selection of change-points in EMG signals, and 6 were not.

All observers were informed about the procedure, and each of them gave a written consent to participate in the experiment. It is worth pointing out that this study was approved by the Ethics Committee of the UAA (permission CIB-UAA-15).

Test signals. We considered signals with 1, 2 and 3 activity phases ($n_{bursts} = 3$), with three possible curve shapes ($n_{sh} = 3$) and two possible SNR ($n_{snr} = 2$) with levels of 20 dB and 10.5 dB. A set of 18

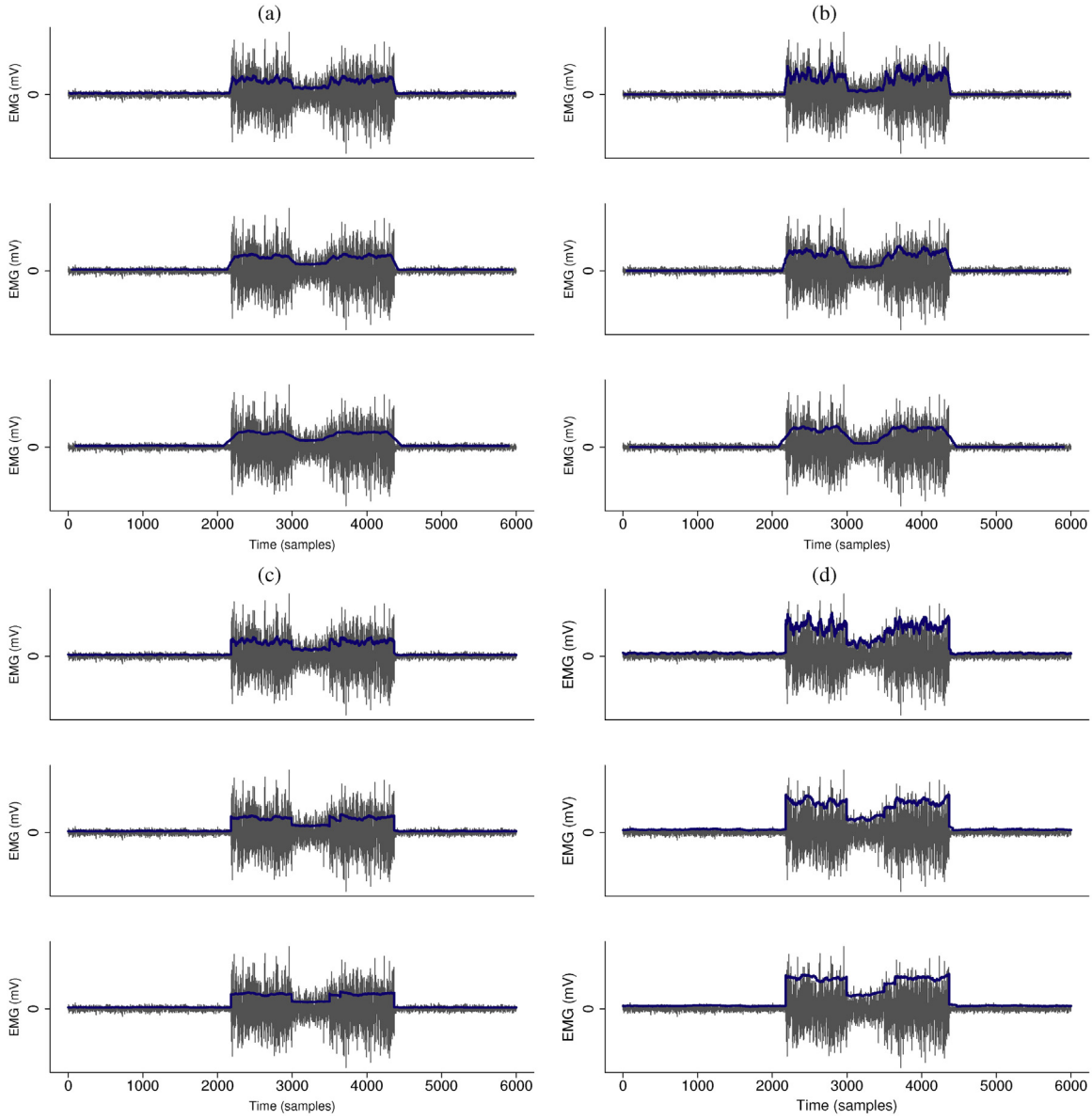

Fig. 3. Effects of the window size in smoothing of the envelope. The envelopes were calculated using (a) moving averages, (b) *MAbs*, (c) root-mean squares and (d) *CIbs*. Each method was implemented using three windows sizes: $w = 10$ (top), $w = 60$ (middle), $w = 100$ (bottom).

synthetic signals ($n_{bursts} \times s_{sh} \times n_{snr}$) was produced beforehand, and their envelopes were computed using the methods *MA*, *RMS*, *MAbs* and *CIbs*), with three different window sizes (21, 81 and 201 samples). In this way, 216 test envelopes were obtained. The original 18 rectified signals were inserted at random in these 216 envelopes to determine if the use of envelopes helps during the process of manual selection. All the envelopes and the rectified signals were stored in a database which was used by all the subjects.

Remark 1. It is worth pointing out that the methods *MAbs* and *CIbs* consider a parameter α which is not present in the other techniques. In our experiments, we set $\alpha = 0.01$. Likewise, the method *LE* was not considered here in view that the set of its parameters is entirely different. All the signals began and ended with a phase of silence. The length of each phase was determined at random, and the resulting signal was cut to 16,000 samples per signal. All the signals had between 1 and 3 phases of activation.

Interface of manual selection. A graphic computer interface was designed for the subjects to select the beginning and ending of activation phases using mouse. The entire computer screen basically showed the complete signal or the envelope of the database. Note that only $2n_f$ or 2 clicks were needed for each phase of activation. At the end of each plot, the computer program immediately switched to the next signal

Experimental setting. All the participants of the experiment worked at the same time and using equipment with similar characteristics. More precisely, they worked on desktop computers, with a Intel Core i5 4590 processor at 3.3 GHz, with a 500 GB hard drive of 16 GB RAM DDR3, using 64-bit Windows 10 Pro as operating system. They used a 21.5 in monitor with 1920 × 1080 pixels resolution. The experiment was divided in 3 sessions of 78 signals each, with a rest between each session. The experiment took approximately 40 min per participant.

Quality measures. We were interested in the precision of the selection of the beginning and ending points of the activity phases,

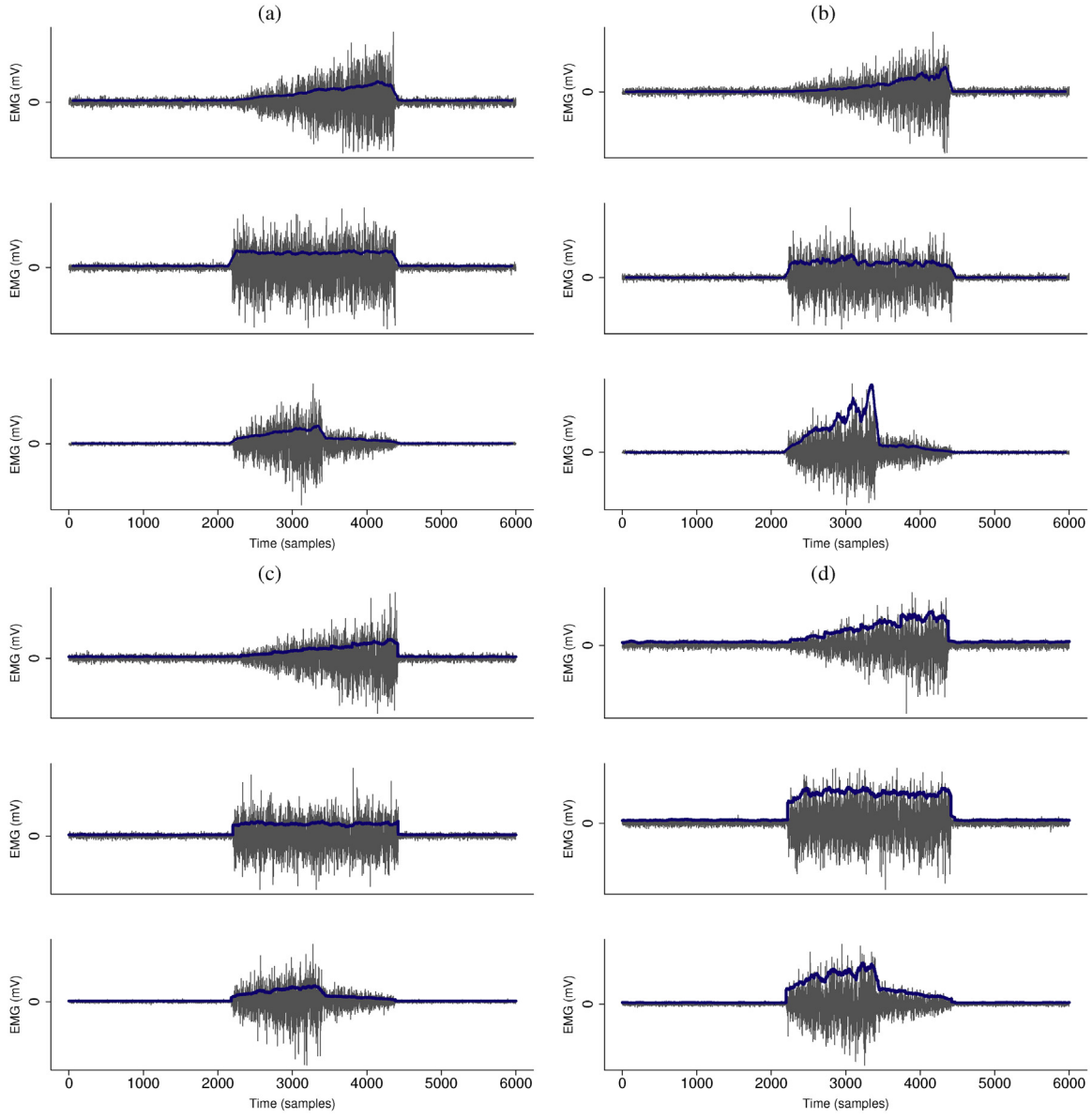

Fig. 4. Shape recovery using four different methods. The envelopes were calculated using (a) moving averages, (b) *MAbs*, (c) root-mean squares and (d) *CIbs*. Each method was implemented using three different shapes and a constant window size $w = 50$.

as well as in the average time to carry out the identifications. As a measure of precision, we used

$$Precision = \frac{\sum_{i=1}^{2n_f} |x_i - \tilde{x}_i|}{2n_f}, \tag{22}$$

where n_f is the number of phases present in the signal, x_i are the true points that the participant had to choose (one at the beginning and one at the end of each phase of activation) and $\tilde{x}_i$ is the point actually chosen by the subject. The units of *Precision* are in samples. To estimate the time required for each point, we divided the total time needed by each subject to process each signal by $2n_f$, that is, the total number of points that the subject had to choose. This measure is called *Mean Time* (per point), and its units are seconds.

4.2.2. Results and discussion

The data corresponding to *Mean Time* and *Precision* were analyzed using a linear ANOVA table with interactions, considering the factors *Shape* (with levels: rectangular, triangular, asymmetric triangular), *Bursts* (number of bursts levels: 1–3), *SNR* (20 dB and 10.5 dB), *WindowL* (window length with levels 21, 81, 201 for envelopes, and a 'dummy' value equal to 1 for rectified signals) and *Method* (for levels *MA*, *RMS*, *MAbs*, *CIbs*, Rectified).

Table 1
Mean Time and average *Precision* for each of the methods to calculate envelopes.

	Method				
	MAbs	CIbs	MA	RMS	Rectified
Mean time	1.89	2.01	1.73	2.09	1.90
Precision	72.52	76.34	105.25	115.39	119.61

In the case of *Mean Time*, the factor *SNR* was not significant (p-value equal to 0.4722314) but the remaining factors were highly significant (the p-values were 4.300×10^{-5}, 6.459×10^{-9}, 3.419×10^{-12}, 1.626×10^{-6} for *Shape*, *Bursts*, *WindowL*, *Method*, respectively). Fig. 7 shows the individual values of *Mean Time* for each of the signals and all the participants. In turn, Table 1 shows the average values per method. We note that, even when there is a statistical difference in favor of the performance of *MA* (followed

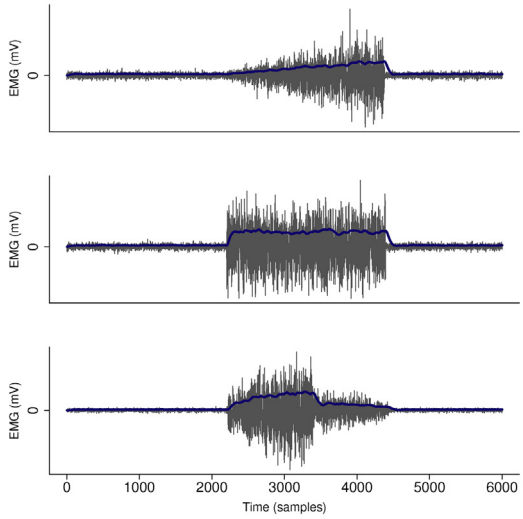

Fig. 5. Shape recovery using the Butterworth low-pass filter, three different shapes and a cut frequency equal to 60 Hz.

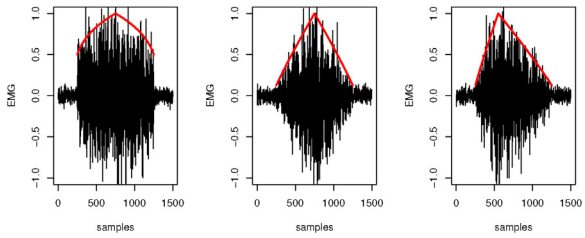

Fig. 6. Examples of different forms of activity phases obtained by varying the signal S_{shape} (solid red line). From left to right: rectangular, triangular form, asymmetric triangular form. (For interpretation of the references to color in text/this figure legend, the reader is referred to the web version of the article.)

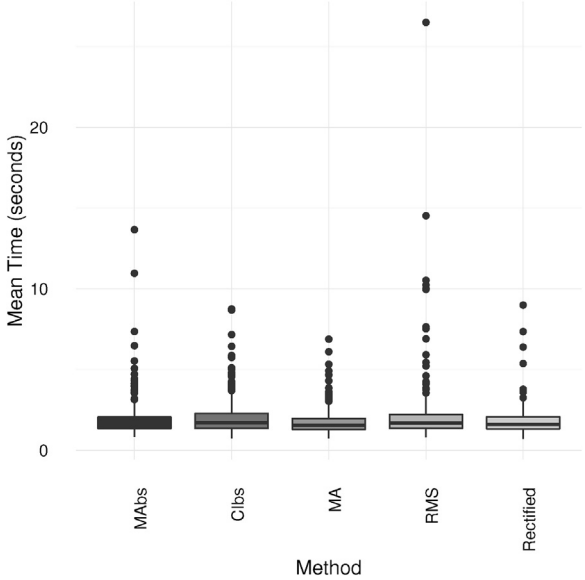

Fig. 7. Individual values of *Mean Time* for each of the methods considered in this work.

closely by *MAbs* and the rectified signal), all the average times are approximately equal to 2 s. Thus, there is no substantial difference between them.

In the case of *Precision*, all the principal factors were significant (*WindowL* with a *p*-value of 0.00017, and the rest of them with a *p*-value less that 2.2×10^{-16}). Fig. 8 shows the individual values of *Precision* for each of the signals and each participant. Meanwhile, Table 1 shows the respective average values per method. Obviously, the use of envelopes improves the precision (the mean error decreases) as compared to the results in which the original rectified signal is employed. Notice that the method presented in this work possess average values of *Precision* which are less than those corresponding to the other methods.

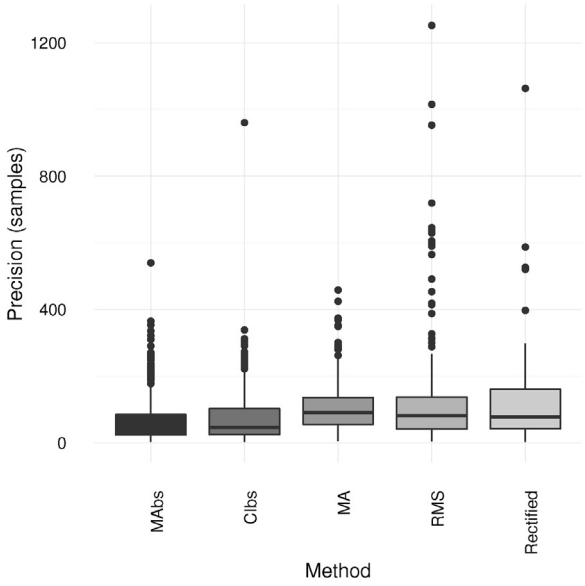

Fig. 8. Individual values of *Precision* for each of the methods considered in this work.

Table 2
Mean values of *Precision* for combinations of various methods for the calculation of envelopes with the parameters. In the case of the rectified signals the factor *WindowL* is not present. In light of this fact, the average value of *Precision* is provided for rectified signals in general.

	Method				
	MAbs	CIbs	MA	RMS	Rectified
Shape					
Rect	31.2	39.8	77.6	64.8	47.5
Triangular	77.5	82.3	107.5	112.7	149.1
assynTriang	108.8	107.0	130.6	168.6	162.2
Bursts					
1	90.8	88.3	116.4	170.0	157.9
2	71.9	73.6	106.8	89.6	101.2
3	54.8	67.2	92.5	86.5	99.7
SNR					
20 dB	36.3	41.1	80.2	103.2	66.4
10.5 dB	108.8	111.6	130.3	127.6	172.8
WindowL					
21	81.4	83.6	85.8	91.0	
81	76.0	85.5	99.1	113.7	119.6
201	60.1	59.9	130.8	141.5	

The interactions of *Method* with the other four factors were significant (*p*-values equal to 0.0201 for *Shape*Method*, 7.263×10^{-7} for *Bursts*Method*, 5.778×10^{-5} for *SNR*Method* and 1.675×10^{-9} for *WindowL*Method*, with the symbol * meaning interaction between the two factors). Fig. 9 shows the individual values for the combination of levels for *Method* and the remaining factors, while Table 2 shows the corresponding mean values. We note the following from those results:

- About the interaction between the factors *Method* and *Shape*, we note that the methods consistently yield better average values. In

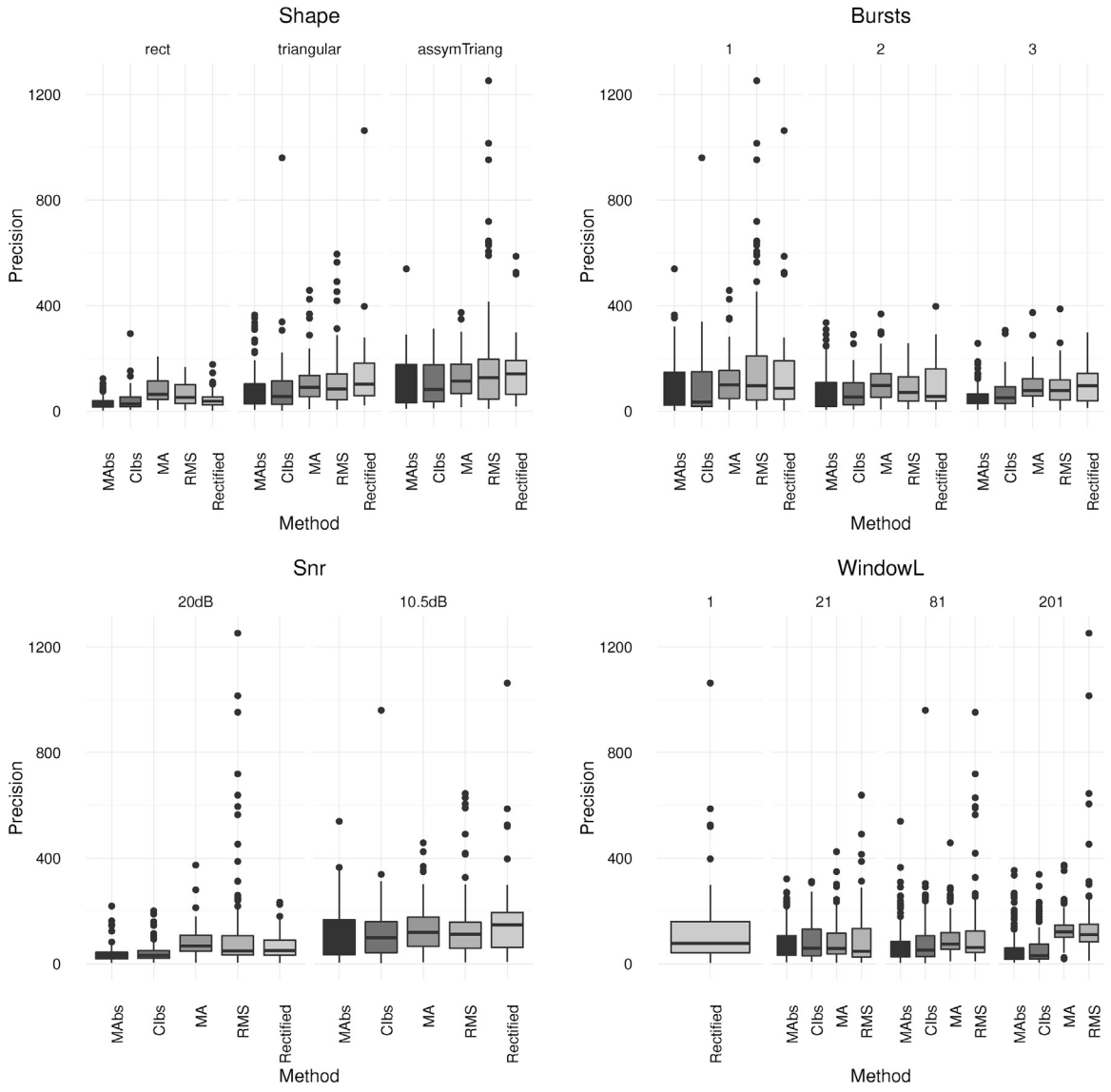

Fig. 9. Individual values of *Precision* for each of the methods considered in this work.

addition, the form of the phase of activation influences the precision. Indeed, the rectangular form has the best average values followed by the triangular, and the asymmetric triangular next. In the case of the rectangular form, it is better to use the rectified signal over the envelopes *MA* and *RMS*.

- With respect to the factors *Method* and *Bursts*, notice that the average precision improves as the number of activation phases increases. This may be due to the fact that the possible position of a point is bounded from above by the position of the next point.
- In the case of the interaction between the factors *Method* and *SNR*, the greater the signal-to-noise ration (that is, the lower the relative magnitude of the phase of silence) the easier it is to decide on the location of the points of interest and the higher the precision. Observe that the methods proposed in this manuscript yield better results. Moreover, we also witness a case in which it is better to use the rectified signal over the methods *MA* and *RMS* (see the case when *SNR* is equal to 20 dB).
- The interaction between the factors *Method* and *WindowL* is especially interesting. Indeed, when the value of *WindowL* increases then the signal is smoothed and the shape of the signal is easier to recognize. For the methods *MA* and *RMS*, such increase implies a loss in the precision, while yielding improvements in the case of the methods proposed in this work.

4.3. Automatic selection

The simplest automatic methods to detect phases of activity are based on the *single threshold scheme*, which consists in calculating an envelope and letting the points of the activity phases be those samples whose envelope value is higher than a certain threshold. In this type of methods, the main concern is to define the optimal threshold value. The present test shows that the proposed envelopes allow to determine this optimal value in an easy way.

4.4. Methodology

There was no need to use subjects for this test in view that the methodology is automatic.

Test signals. We considered signals with three phases of activation, three forms of the activation phases (rectangular, triangular, asymmetric triangular) with 10.5 dB and 20 dB of SNR. In total, there are 6 types of signals. A set of 100 synthetic signals of each

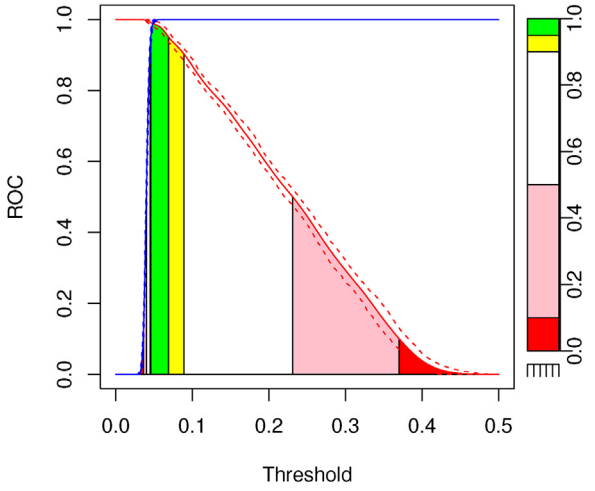

Fig. 10. Average ROC curves $\bar{SEN}$ (red) and $\bar{SPE}$ (blue), with empirical 90% confidence intervals (dashed). The graph shows also the regions corresponding to values of $\bar{SEN}$ an $\bar{SPN}$ which are greater than 0.95 (green), between 0.90 and 0.95 (yellow), less than 0.50 (pink) and strictly less that 0.10 (red). (For interpretation of the references to color in text/this figure legend, the reader is referred to the web version of the article.)

type was generated, and their corresponding envelopes were calculated using each of five methods (n*MA*, *RMS*, *LE*, *MAbs*, *CIbs*). The envelopes were calculated using sequentially sizes of window equal to 3, 5, 9, 13, 21, 35, 55, 91, 149, 245, 405, 667, 1097, 1809 and 2981 (which are approximately equally spaced in a logarithmic scale) for the methods *MA*, *RMS*, *MAbs* and *CIbs*. In the case of *CIbs*, we used $\alpha = 0.05$ and $\alpha = 0.01$, to observe also the effect of this parameter in the determination of the optimal threshold value. Likewise, the cutoff frequency for the method *LE* was sequentially inspected using the values 0.5, 1, 1.6, 2.7, 4.5, 7.4, 12.2, 20.1, 33.1, 54.6, 90.0, 148.4 and 200 Hz (considering that the signals have a sampling frequency equal to 1000 Hz). Again, these values are approximately equally spaced in a logarithmic scale.

Test values for the threshold. The synthetic signals had values between −1 and 1, so that the envelope took on values in [0, 1]. We tested threshold values between 0 and 0.5 using a step-size equal to 0.001 (in total, 501 threshold values).

Quality measures. The purpose of the single threshold scheme is to classify each sample as active (if it belongs to a phase of activity) or silent (if it belongs to a phase of silence). In each of the following definitions, we will consider the particular case of the 100 envelopes corresponding to the synthetic signals with rectangular activation phase and *SNR* equal 20 dB, using the method *MAbs* with window size of *WindowL=81* and $\alpha = 0.01$ (that is, we fix the type of signal and the type of envelope). For each envelope e_i with $i \in \{1, \ldots, 100\}$ and each threshold value t, we calculate

- Number of true-positives ($TP_{t,i}$), that is the number of samples correctly marked as active for the envelope e_i using the threshold value t.
- Number of false-positives ($FP_{t,i}$), that is the number of samples incorrectly marked as active for the envelope e_i using the threshold value t.
- Number of true-negatives ($TN_{t,i}$), that is the number of samples correctly marked as silence for the envelope e_i using the threshold value t.
- Number of false-negatives ($FN_{t,i}$), that is the number of samples incorrectly marked as silence for the envelope e_i using the threshold value t.

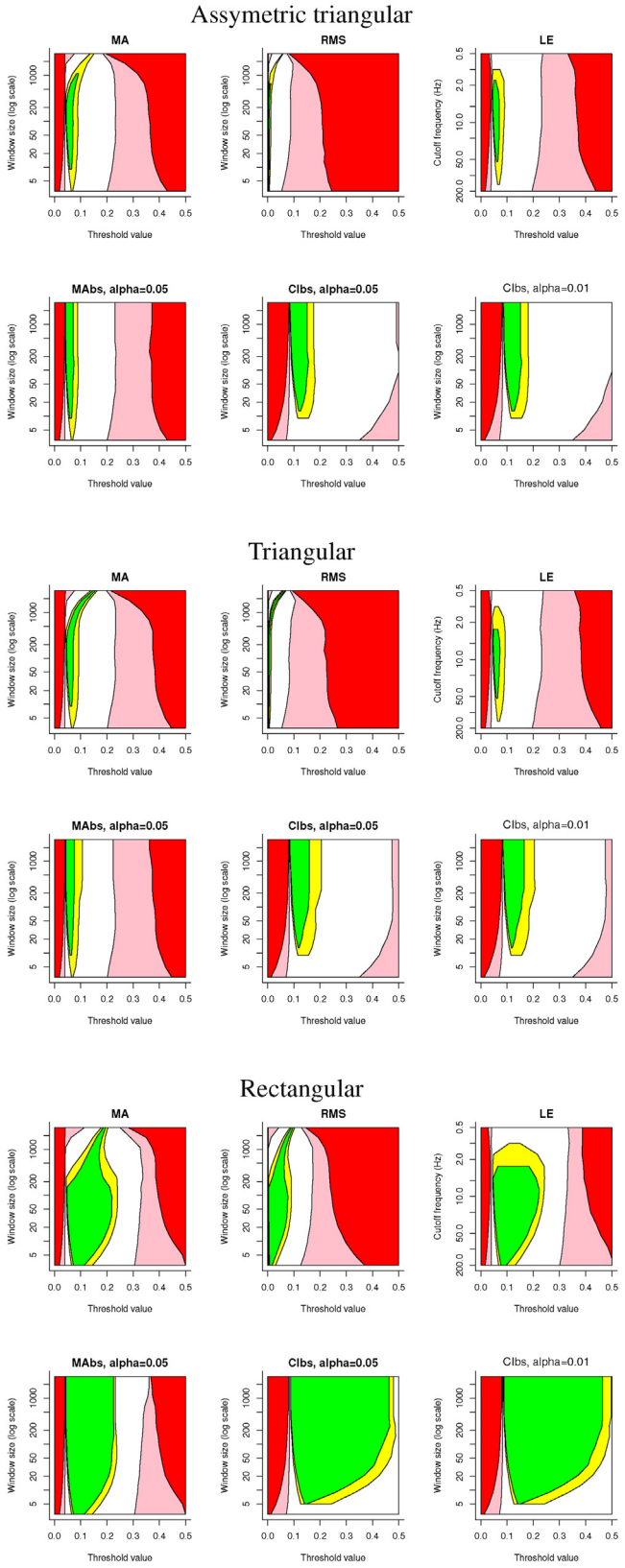

Fig. 11. Favorable regions for signals with *SNR* equal to 20 dB. We considered the different parameter spaces of the method investigated in this work. The color scale is the same as that used in Fig. 10. (For interpretation of the references to color in text/this figure legend, the reader is referred to the web version of the article.)

Based on this values, we define the sensitivity or the true-positive rate as

$$SEN_{t,i} = \frac{TP_{t,i}}{TP_{t,i} + FN_{t,i}}, \tag{23}$$

and the specificity or true-negative rate as

$$SPE_{t,i} = \frac{TN_{t,i}}{TN_{t,i} + FP_{t,i}}. \tag{24}$$

These last quantities define ROC curves in terms of t which depend on the envelope e_i. Using the fact that 100 signals of each kind were simulated, and that an envelope was calculated for each of them using fixed values of the parameters, we can define the average ROC curves

$$\bar{SEN}_t = \frac{\sum_{i=1}^{100} SEN_{t,i}}{100} \tag{25}$$

and

$$\bar{SPE}_t = \frac{\sum_{i=1}^{100} SPE_{t,i}}{100} \tag{26}$$

4.4.1. Results and discussion

Fig. 10 shows the ROC curves $\bar{SEN}_t$ and $\bar{SEN}_t$. These figures also depict empirical confidence intervals for the curves. The results show that these average curves are good representatives of the 100 curves used to calculate them. It is worth pointing out that the classification strives for the sensitivity and the specificity to have high values. The result for this example show that a suitable value for the threshold would be 0.06 in view that the sensitivity and the specificity are greater thane 0.95 for such threshold value. As a reference, we have highlighted the regions corresponding to values of $\bar{SEN}$ and $\bar{SPE}$ greater than 0.95 (green), between 0.90 and 0.95 (yellow), less than 0.50 (pink) and less that 0.10 (red). The desirable threshold values are found within the green and the yellow regions, while the worse choices are between the pink and the red regions.

The analysis of the previous paragraph was carried out for a window size of 81. Figs. 11 and 12 show the behavior when this parameter is varied. Those figures show level curves in the space of parameters for each of the methods considered in this work, for both $\bar{SEN}$ and $\bar{SPE}$. The color levels are the same as those of Fig. 10.

We must point out that, in all the cases, the regions of favorable parameters (yellow and green) are wider along the horizontal axis for the method *CIbs* (this is true for the two values of α considered). This means that, given an envelope with parameter *windowL*, there are more threshold values which yield good results in terms of sensitivity and specificity, which means that the value of that parameter would be easy to adjust. For some values of *WindowL*, the favorable regions have equal width for *MAbs* and *MA*. However, for the method *MA*, the favorable regions become more narrow as the window size increases. The opposite situation is observed for *MAbs*. The same phenomenon happens for the methods *RMS* (which has the narrowest regions) and *LE*. We also notice that the favorable regions are wider if the *SNR* increases or if the shape has a smoother contour, as expected.

4.5. Real data

Beforehand, we must point out that synthetic and real signals shows similar qualitative outcomes. Figs. 14 and 15 show the results obtained using the five envelope methods for a real signal of the motion of a human biceps (see Fig. 13). More precisely, Fig. 14 shows the results obtained using (a) moving averages, (b) *MAbs*, (c) root-mean squares and (d) *CIbs*; meanwhile Fig. 15 was obtained using the Butterworth lower-pass filter. Note that the methods of

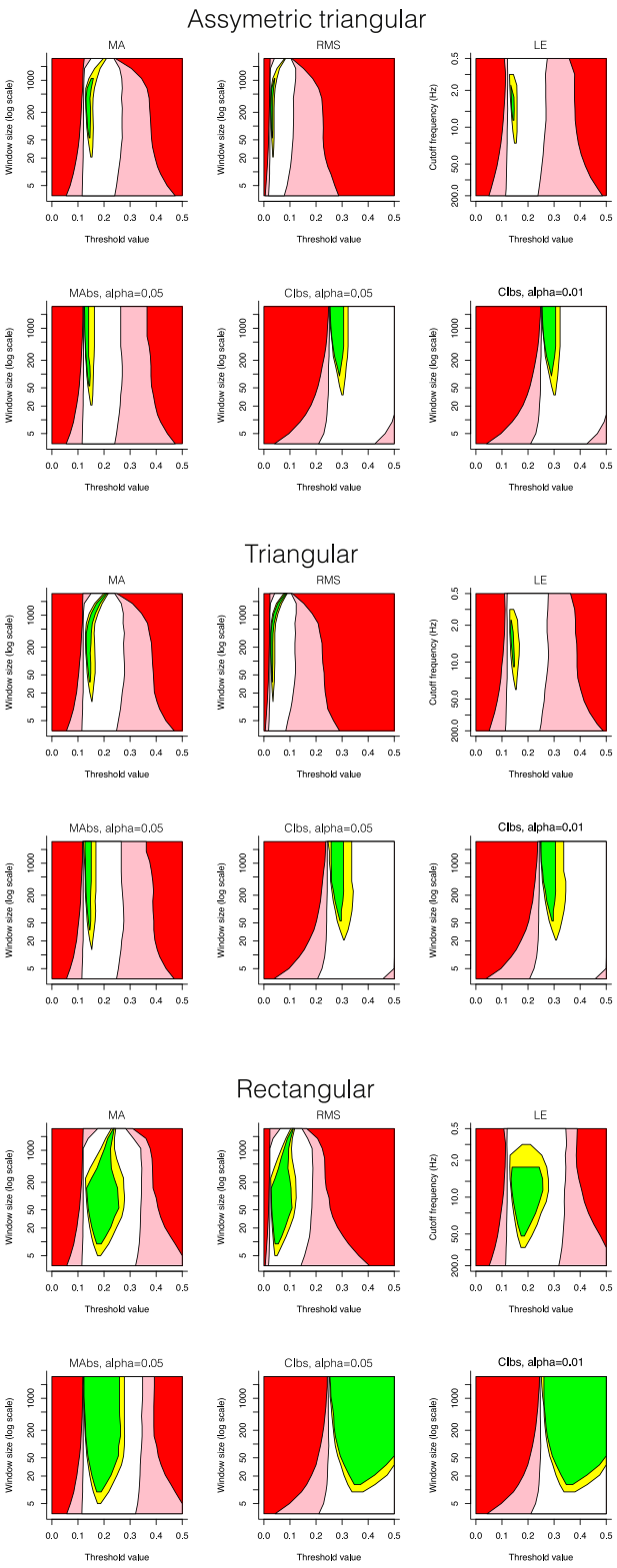

Fig. 12. Favorable regions for signals with *SNR* equal to 10 dB. We considered the different parameter spaces of the method investigated in this work. The color scale is the same as that used in Fig. 10. (For interpretation of the references to color in text/this figure legend, the reader is referred to the web version of the article.)

Fig. 13. Arm motion to obtain real biceps EMG signals. The arm of the subject is initially at rest and holding a weight of 4 kg, with the elbow touching the body (left). The subject then lifts the weight with the elbow touching the body (center). Finally, the arm returns to the original resting position (right). This motion is repeated three times.

moving averages and root-mean squares miss the shape of the signal as the window size increases. A similar effect occurs with the Butterworth low-pass filter when the cut frequency is decreased. Also, note that these two methods miss the starting points of the bursts. On the other hand, the method *MAbs* can fully retrieve the starting and ending point of the burst along with the shape of the signal. Similarly *CIbs* can retrieve the shape and the amplitude of the signal. It is worthing recalling that the amplitude is a useful parameter in electromyography to determine how many muscle fibers are fired up at once [26].

5. Conclusions

In this work, we have proposed two novel methods (named *MAbs* and *CIbs*) to retrieve the shape and the amplitude of the bursts of sEMG signals. The proposed methods identify the start and end of bursts when other traditional methods cannot. Our comparisons were performed against the techniques of moving averages, root-mean squares and Butterworth low-pass filters using both real and synthetic signals. In particular, it is worth pointing out that the

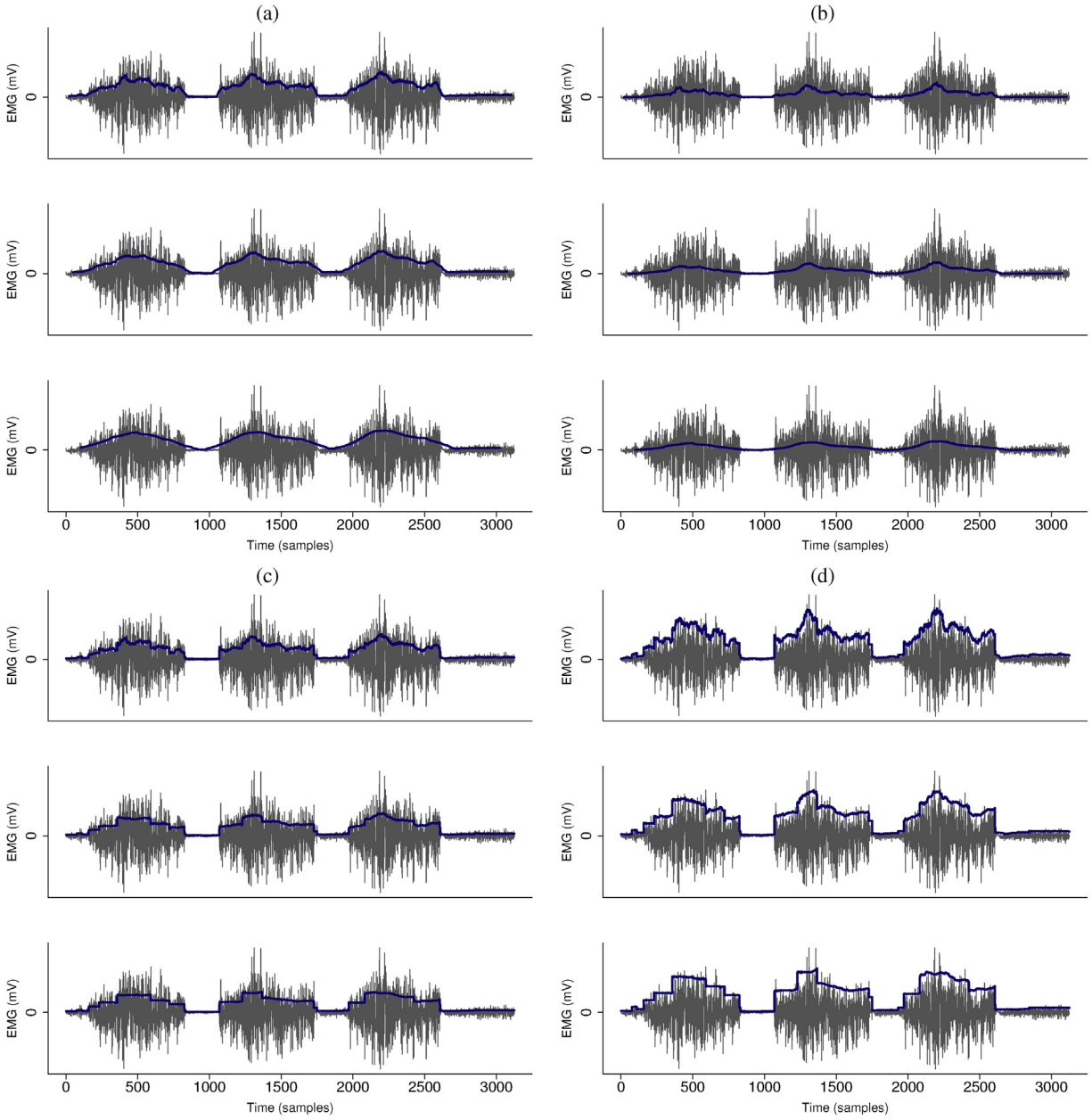

Fig. 14. Envelope computed using four methods. The envelopes were calculated using (a) moving averages, (b) *MAbs*, (c) root-mean squares and (d) *CIbs*. Each method was implemented using three windows sizes: $w = 10$ (top), $w = 60$ (middle), $w = 100$ (bottom). Amplitude is retrieved by *CIbs*, and shape by both *CIbs* and *MAbs*.

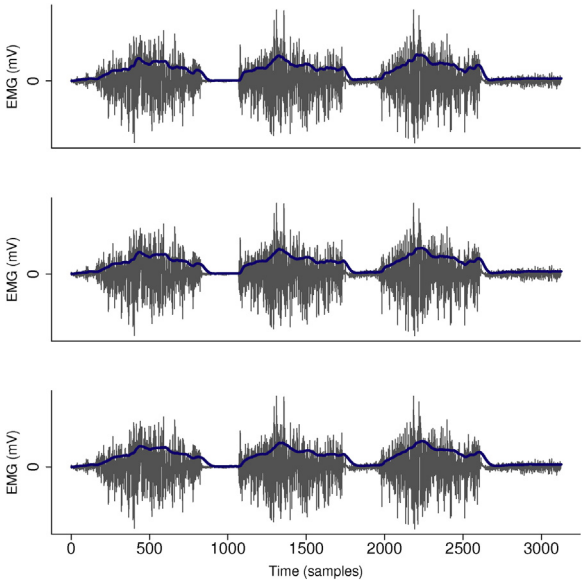

Fig. 15. Envelope computed using the Butterworth lower-pass filter and three cut frequencies: 60 Hz (top), 55 Hz (middle), 50 Hz (bottom).

shape calculated through *CIbs* gets an estimation of the amplitude for each point in the signal.

It is important to point out that the methods proposed in this manuscript consider the presence of some quantitative parameters that may be tuned up to retrieve the shape, the peaks, the valleys and the jumps required in a wide range of EMG signal processing applications. In particular, the envelope can be as smooth as desired without losing the precision of the localization of the start and end of bursts. The methods were thoroughly validated using a wide range of experiments with real and synthetic data.

Acknowledgements

The authors wish to thank the anonymous reviewers and the associate editor in charge of handling this manuscript for all their invaluable comments. Their criticisms and suggestions helped in improving the quality of this work.

References

[1] A. Subasi, Classification of EMG signals using PSO optimized SVM for diagnosis of neuromuscular disorders, Comput. Biol. Med. 43 (5) (2013) 576–586.
[2] J. Halford, D. Cardenas, L. Whitmire, J. Cavazos, M. Girouard, Application of sEMG feature extraction from EEG recordings for evaluation of generalized tonic–clonic seizure semiology, Neurology 8 (16 Suppl) (2017) 2–224.
[3] J. Selvaraj, M. Murugappan, W. Khairunizam, W. Ahmad, Y. Sazali, Emotion recognition from facial EMG signals using higher order statistics and principal component analysis, J. Chin. Inst. Eng. 37 (3) (2014) 385–394.
[4] S. Amsuss, P.M. Goebel, N. Jiang, B. Graimann, L. Paredes, D. Farina, Self-correcting pattern recognition system of surface EMG signals for upper limb prosthesis control, IEEE Trans. Biomed. Eng. 61 (4) (2014) 1167–1176.
[5] A. Schmitz, A. Silder, B. Heiderscheit, J. Mahoney, D.G. Thelen, Differences in lower-extremity muscular activation during walking between healthy older and young adults, J. Electromyogr. Kinesiol. 19 (6) (2009) 1085–1091.
[6] C. McNee, J. Kieser, J. Antoun, H. Bennani, L. Gallo, M. Farella, Neck and shoulder muscle activity of orthodontists in natural environments, J. Electromyogr. Kinesiol. 23 (3) (2013) 600–607.
[7] S.A. Ferguson, W.G. Allread, P. Le, J. Rose, W.S. Marras, Shoulder muscle fatigue during repetitive tasks as measured by electromyography and near-infrared spectroscopy, Hum. Fact. 55 (6) (2013) 1077–1087.
[8] P. Konrad, The ABC of EMG, A Practical Introduction to Kinesiological Electromyography, vol. 1, 2005, pp. 30–35.
[9] H. Kalani, S. Moghimi, A. Akbarzadeh, SEMG-based prediction of masticatory kinematics in rhythmic clenching movements, Biomed. Signal Process. Control 20 (2015) 24–34.
[10] J. Barrios-Muriel, F. Romero, F.J. Alonso, K. Gianikellis, A simple SSA-based de-noising technique to remove ECG interference in EMG signals, Biomed. Signal Process. Control 30 (2016) 117–126.
[11] E. Gokgoz, A. Subasi, Comparison of decision tree algorithms for EMG signal classification using DWT, Biomed. Signal Process. Control 18 (2015) 138–144.
[12] Y. Ji, S. Sun, H.-B. Xie, Stationary wavelet-based two-directional two-dimensional principal component analysis for EMG signal classification, Meas. Sci. Rev. 17 (3) (2017) 117–124.
[13] M. Esquivel-Frausto, J.A. Guerrero, J.E. Macías-Díaz, Activity pattern detection in electroneurographic and electromyogram signals through a heteroscedastic change-point method, Math. Biosci. 224 (2) (2010) 109–117.
[14] J.A. Guerrero, J.E. Macías-Díaz, A computational method for the detection of activation/deactivation patterns in biological signals with three levels of electric intensity, Math. Biosci. 248 (2014) 117–127.
[15] C. Wu, Y. Zhang, C. Hong, H. Chiueh, Implementation of ECG signal processing algorithms for removing baseline wander and electromyography interference, Communication Software and Networks (ICCSN), 2016 8th IEEE International Conference on, IEEE (2016) 118–121.
[16] N. Miljković, N. Popović, O. Djordjević, L. Konstantinović, T.B. Šekara, ECG artifact cancellation in surface EMG signals by fractional order calculus application, Comput. Methods Progr. Biomed. 140 (2017) 259–264.
[17] S. Benatti, G. Rovere, J. Bösser, F. Montagna, E. Farella, H. Glaser, P. Schönle, T. Burger, S. Fateh, Q. Huang, et al., A sub-10 mW real-time implementation for EMG hand gesture recognition based on a multi-core biomedical SoC, Advances in Sensors and Interfaces (IWASI), 2017 7th IEEE International Workshop on, IEEE (2017) 139–144.
[18] A. Alkan, M. Günay, Identification of EMG signals using discriminant analysis and SVM classifier, Expert Syst. Appl. 39 (1) (2012) 44–47.
[19] Y. Yun, S. Dancausse, P. Esmatloo, A. Serrato, C.A. Merring, P. Agarwal, A.D. Deshpande, Maestro: an EMG-driven assistive hand exoskeleton for spinal cord injury patients, Robotics and Automation (ICRA), 2017 IEEE International Conference on, IEEE (2017) 2904–2910.
[20] A. Akhtar, Estimation of distal arm joint angles from EMG and shoulder orientation for transhumeral prostheses, Ph.D. thesis), 2016.
[21] A.d.S. Ferreira, F.S. Guimarães, M.A.R. Magalhães, et al., Accuracy and learning curves of inexperienced observers for manual segmentation of electromyograms, Fisioterapia em Movimento 26 (3) (2013) 559–567.
[22] A. de Sá Ferreira, F. Silva Guimaraes, R. Coeli Souza e Silva, M.A. Ribeiro Magalhaes, Effects of supervised practice on the accuracy of observers for manual segmentation of simulated electromyograms, Kinesiology 46 (2) (2014) 171–178.
[23] S.S. Wilks, The large-sample distribution of the likelihood ratio for testing composite hypotheses, Ann. Math. Stat. 9 (1) (1938) 60–62.
[24] M. Csörgö, L. Horváth, Limit Theorems in Change-point Analysis, vol. 18, John Wiley & Sons Inc., New York, 1997.
[25] L.J. Vostrikova, Detecting disorder in multidimensional random processes, Soviet Math. Doklady 24 (1981) 55–59.
[26] G.L. Gottlieb, G.C. Agarwal, Dynamic relationship between isometric muscle tension and the electromyogram in man, J. Appl. Physiol. 30 (3) (1971) 345–351.